A Numerical Simulation of Vortex Induced Vibration on a Elastically Supported Circular Rigid Cylinder at Moderate Reynolds Numbers

Jean-François Sigrist, Cyrille Allery, Claudine Beghein

▶ **To cite this version:**

Jean-François Sigrist, Cyrille Allery, Claudine Beghein. A Numerical Simulation of Vortex Induced Vibration on a Elastically Supported Circular Rigid Cylinder at Moderate Reynolds Numbers. ASME, Pressure Vessel and Pipiping Conference (PVP 2008), Jul 2008, Chicago, United States. pp.83-92, 10.1115/PVP2008-61003 . hal-04642660

HAL Id: hal-04642660
https://hal.science/hal-04642660

Submitted on 19 Jul 2024

HAL is a multi-disciplinary open access archive for the deposit and dissemination of scientific research documents, whether they are published or not. The documents may come from teaching and research institutions in France or abroad, or from public or private research centers.

L'archive ouverte pluridisciplinaire **HAL**, est destinée au dépôt et à la diffusion de documents scientifiques de niveau recherche, publiés ou non, émanant des établissements d'enseignement et de recherche français ou étrangers, des laboratoires publics ou privés.

Proceedings of PVP2008
2008 ASME Pressure Vessels and Piping Division Conference
July 27-31, 2008, Chicago, Illinois, USA

A NUMERICAL SIMULATION OF VORTEX INDUCED VIBRATION ON A ELASTICALLY SUPPORTED CIRCULAR RIGID CYLINDER AT MODERATE REYNOLDS NUMBERS

Jean-François SIGRIST
Service Technique et Scientifique
DCNS Propulsion
44620 LA MONTAGNE, France
jean-francois.sigrist@dcnsgroup.com

Cyrille ALLERY, Claudine BEGHEIN
Laboratoire d'Etude des Phénomènes de Transfert Appliqués au Bâtiment
Université de La Rochelle
17000 LA ROCHELLE France
callery@univ-lr.fr, cbeghein@univ-lr.fr

ABSTRACT

The present paper is the sequel of a previously published study which is concerned with the numerical simulation of vortex-induced-vibration (VIV) on an elastically supported rigid circular cylinder in a fluid cross-flow (A. Placzek, J.F. Sigrist, A. Hamdouni; Numerical Simulation of Vortex Shedding Past a Circular Cylinder at Low Reynolds Number with Finite Volume Technique. Part I: Forced Oscillations, Part II: Flow Induced Vibrations; Pressure Vessel and Piping, San Antonio, 22-26 July 2007). Such a problem has been thoroughly studied over the past years, both from the experimental and numerical points of view, because of its theoretical and practical interest in the understanding on flow-induced vibration problems. In this context, the present paper aims at exposing a numerical study based on a fully coupled fluid-structure simulation. The numerical technique is based on a finite volume discretisation of the fluid flow equations together with i) a re-meshing algorithm to account for the cylinder motion ii) a projection subroutine to compute the forces induced by the fluid on the cylinder and iii) a coupling procedure to describe the energy exchanges between the fluid flow and solid motion. The study is restricted to moderate Reynolds numbers (R_e~2.000-10.000) and is performed with an industrial CFD code. Numerical results are compared with existing literature on the subject, both in terms of cylinder amplitude motion and fluid vortex shedding modes. Ongoing numerical studies with different numerical techniques, such as ROM (Reduced Order Models)-based methods, will complete the approach and will be published in next PVP conference. These numerical simulations are proposed for code validation purposes prior to industrial applications in tube bundle configuration.

INTRODUCTION

Flow past an oscillating cylinder becomes unstable for Reynolds numbers beyond R_e~47 and the cylinder therefore experiences unsteady hydrodynamic forces which result from the vortex shedding process. Motion of the cylinder induced by the unsteady forces alters in response the fluid flow field and the vortex shedding. Under some particular condition, the vortex shedding frequency can be tuned to the natural frequency of the oscillating cylinder: this fluid-structure coupling phenomenon is often referred to as "synchronization" or "lock-in"[1] and is one of the most striking example of Vortex-Induced Vibrations (VIV) [2,3]. It can be encountered in numerous industrial situations, for instance in civil engineering (bridges, chimney stacks), in marine engineering (power transmission lines, marine towing cables) or even in nuclear engineering (heat exchangers, tube bundles). In propulsion systems, VIV is also the cause of structural vibrations (rudders, propellers) associated with sound radiation and/or fatigue phenomenon and has therefore to be accounted for in the design process.

VIV has therefore received a lot of attention over the past decades, both from the engineers and researchers: early fundamental studies on the subject can be found for instance in the comprehensive review of Sarpkaya [19] as well as in the books of Blevins [2] and Chen [3]. A lot of experimental studies have also been conducted since the pioneer experiments of Feng [5], to the latest work of Govardhan and Williamson [7]. With the development of computer technology, VIV has also been extensively investigated by means of numerical simulations, including RANS (Reynolds Averaged Navier-Stokes), LES (Large Eddy Simulations),

[1] *Definition of "lock-in" as a simple matching of the vortex shedding frequency and the cylinder natural frequency refers to a rather crude description of the process. A thorough discussion on the "true" definition of lock-in is developed by Govardhan & Williamson [7] or Khalak & Williamson [12], to which the reader is invited to refer for a deeper insight on the phenomenon.*

DNS (Direct Numerical Simulations) approaches with DVM (Discrete Vortex Method), FEM (Finite Element Method) or FVM (Finite Volume Method), in 2D and 3D configurations; an extended bibliography on the subject is beyond the scope of the present paper, which only gives a few references on the matter [1,4,8,15,16,18,21,22,26,28][2].

In the present paper, numerical simulations of VIV at moderate Reynolds numbers (R_e~2.000-10.000) for a circular cylinder at low m^*-ζ parameter are performed using a CFD code with RANS equations. The main result of the present study is that the so-called "upper branch" response of the cylinder has been simulated for cylinder let free to oscillate from rest in the transverse direction; to the authors' knowledge, such a result has never been reported in previous numerical studies[3].

The paper is organized as follows: in the first section, various features of VIV for cylinders with low mass-damping parameters are recalled; in the second section, basic principles of the numerical approach employed in the present simulations are exposed; in the third section, numerical results are discussed by comparison with experimental data available in the literature, both in terms of cylinder oscillation amplitude and frequency as well as in terms of vortex shedding mode.

Relative agreement between numerical simulations and experimental observations yield promising results and give confidence in the use of CFD analysis for engineering applications.

1. VORTEX-INDUCED VIBRATION ON A ELASTICALLY MOUNTED RIGID CYLINDER

Figure 1 depicts the case under study in the present paper: one considers a rigid circular cylinder of diameter D, length H and mass m let free to oscillate on its elastic support (with stiffness k and damping c) in the direction transverse to a fluid of density ρ and viscosity μ with upstream velocity U.

When vortex shedding occurs, fluid forces on the cylinder become unsteady and the transverse (or "lift") component of the force φ_L induces motion of the cylinder y, governed by the dynamic equation:

$$m\ddot{y} + c\dot{y} + ky = \varphi_L \qquad (1)$$

The latter equation can be re-written in a non-dimensional form using the non-dimensional ratios defined in Tab. 1:

$$\frac{d^2Y}{dt^{*2}} + \frac{4\pi\zeta}{U^*}\frac{dY}{dt^*} + \frac{4\pi^2}{U^{*2}}Y = \frac{2C_L}{\pi m^*} \qquad (2)$$

where $t^* = \frac{tU}{D}$ is the non-dimensional time, $Y = y/D$ is the non-dimensional displacement and $C_L = \frac{\varphi_L}{1/2\rho U^2 DH}$ is the lift coefficient.

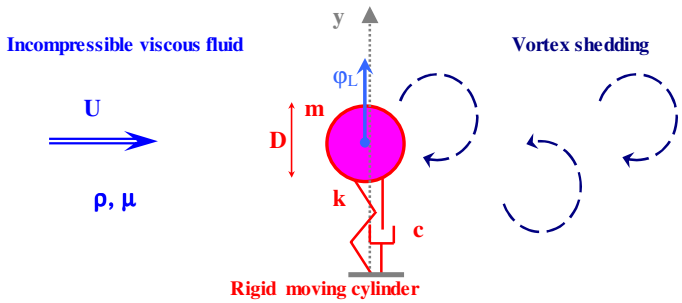

Fig. 1. Elastically mounted rigid cylinder in fluid cross-flow: vortex-induced vibration

As can be inferred from Eq. (2), amplitude of the cylinder oscillation depends *a priori* on the mass ratio m^* and damping ratio ζ and/or a combination of both ratios. Experiments conducted by Feng in 1968 [5] were concerned with VIV in a "light" fluid, i.e. with high mass ratio $m^*=\mathcal{O}(100)$, and a typical cylinder response is represented by Fig. 2, extracted from [12]; in such a case the cylinder maximum amplitude can reach 60% of the cylinder diameter, but the "lock-in" range (i.e. the range of reduced velocity for which "resonant" behavior of the cylinder response under flow forcing is observed) is rather narrow.

Non-dimensional ratio	Symbol	Definition
Mass ratio	m^*	$\frac{m}{\rho\pi D^2 H/4}$
Damping ratio	ζ	$\frac{c}{2\sqrt{k(m+\rho\pi D^2 H/4)}}$
Velocity ratio (*)	U^*	$\frac{U}{f_N D}$
Amplitude ratio	A^*	$\frac{\max_{t>0}(y(t))}{D}$
Frequency ratio (*)	f^*	$\frac{f}{f_N}$
Reynolds number	R_e	$\frac{\rho UD}{\mu}$

Tab. 1. Non-dimensional ratios
(*) f_N *is the natural frequency of the cylinder* <u>*in water*</u>

[2] *The reader is invited to refer to acknowledged journals such as* Computers & Fluids *and* Journal of Fluids & Structures *for an overview on the numerous numerical studies on the subject.*

[3] *Previous studies by Guilmineau & Queutey [8] as well as Pan et* al. *[16], to which the present study will refer, have also presented numerical results yielding the "upper branch" response regime of the oscillating cylinder, but* <u>*not*</u> *with "from rest" initial conditions of motion of the cylinder; reaching the "upper branch" through simulations with a "from rest" initial condition is therefore the major contribution of the present work.*

Design guidelines were deduced from numerical/experimental studies which have been conducted in the sequel of Feng's early experiments for applications in civil engineering for instance, accounting for wind/structure interaction.

Complementary investigations have been carried out for lower mass ratios, which correspond to applications in offshore engineering for instance, and yielded some different behavior: experiments conducted by Khalak & Williamson in 1997 [12] in a "heavy" fluid, i.e. with high mass ratio $m^*=\mathcal{O}(1)$ showed that the cylinder response exhibited higher amplitude response regime with broader extension of the "lock-in" range, see Fig. 2, highlighting a clear effect of the mass ratio on the cylinder response.

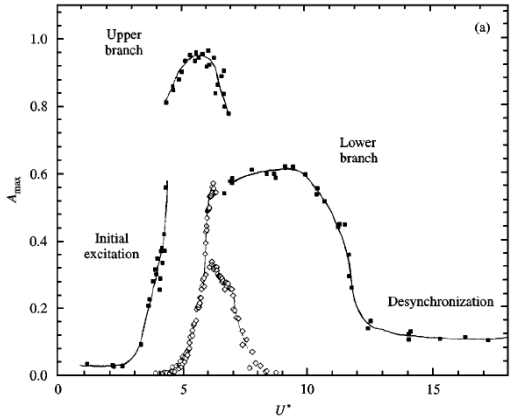

Fig. 2. Cylinder amplitude response from experiments conducted by Khalak & Williamson (1997) ■:m^*=2.4 and Feng (1968) ◊:m^*=268 (from Khalak & Williamson [12])

Khalak & Williamson also investigated the effect of the combined "mass-damping" parameter m^*-ζ and evidenced two types of responses, see Fig. 3, extracted from [12]:

- for high m^*-ζ, the cylinder response is characterized by two modes of response, the so-called "initial excitation branch" and the "lower branch". Maximum amplitude reached in such a case is around 60% of the cylinder diameter, as made conspicuous in Feng's experiments. Furthermore, a hysteretic behavior in the initial↔lower branch transition is observed with respect to the initial conditions in terms of reduced velocity U^*,
- for low m^*-ζ, the cylinder response is characterized by three modes of response, namely the "initial excitation branch", the "upper branch" and the "lower branch". Maximum amplitude reached in such a case is around 90% of the cylinder diameter, as observed in Khalak & Williamson's experiments. Transitions between the initial and upper branches have been found to be hysteretic, while intermittent switching between the "upper branch" and "lower branch" is observed in the "synchronization" regime.

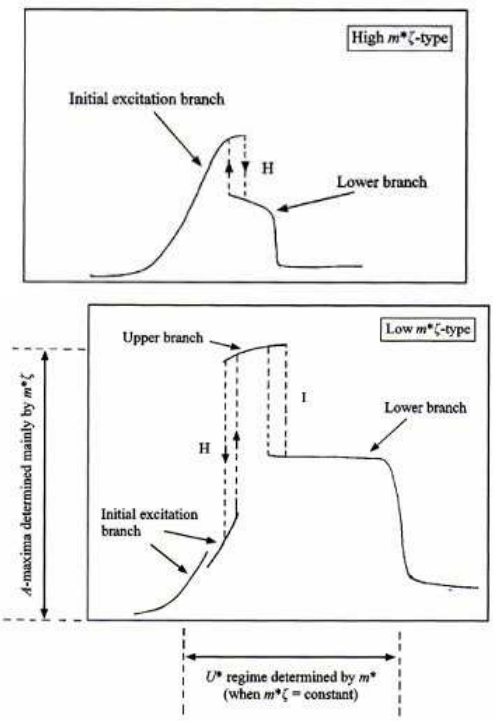

Fig. 3. Amplitude of cylinder vibration under vortex shedding excitation: high and low $m^*\zeta$-type responses (from Khalak & Williamson [12])

Khalak & Williamson's experiments also evidenced that the "synchronization regime" extent is driven by the mass ratio: the lower m^* is, the more extended U^* range for "lock-in" is (this can be also observed in numerical simulations: Shiels et *al.* found a mass ratio-dependency of the "lock-in" zone extend for a circular cylinder at low m^*-ζ and low R_e flow regime, as conveyed by Fig. 4 below, extracted from [21]).

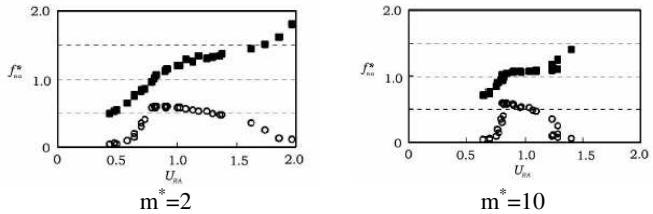

m^*=2 m^*=10

Fig. 4. Lock-in range for low (m^*=2) and high (m^*=10) mass ratios (from Shiels et *al.* [21])

At "resonance" or "lock-in", the cylinder experiences a periodic motion, which can be defined by a frequency ratio f^*, formed as the ratio of the observed cylinder frequency to the cylinder natural frequency in the fluid (according to non-dimensional ratios given in Tab. 1 and [12]). In the experiments conducted at high mass ratios, it was observed

that the frequency of vortex shedding matched the natural frequency of the cylinder and collapsed with the frequency of cylinder oscillations, so that $f^* \approx 1$. "Synchronization" or "lock-in" has therefore long been characterized by equality of the frequency ratio with unity. However, as made conspicuous by Govardhan & Williamson's experiments in 2000 [7] and noted by several authors before, resonance with frequency ratios departing from unity can be observed at low mass ratios. Govardhan & Williamson clarified this mass ratio-dependency of the frequency ratio at resonance and highlighted that i) the velocity ratio range at resonance was all the more extended as the mass ratio was low and ii) the frequency ratio at resonance was all the greater than unity as the mass ratio was low, see Fig. 5, extracted from [7].

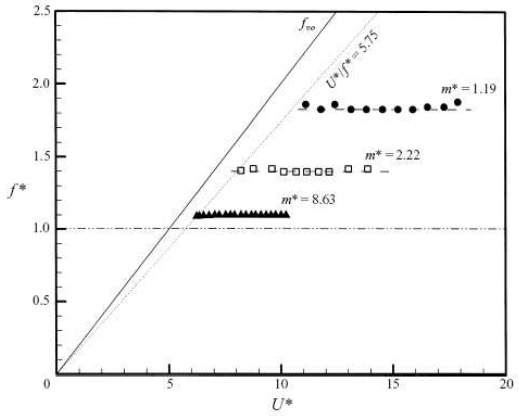

Fig. 5. Reduced frequency f^* at "resonance" as a function of mass ratio m^* (from Govardhan &Williamson [7])

Behavior of the cylinder undergoing VIV is experimentally demonstrated to be radically different at low mass (m^*) and mass-damping (m^*-ζ) ratios; the growing industrial concerns in marine and offshore engineering have therefore encouraged numerical simulations of VIV under these conditions: question of the oscillation amplitude of a cylinder experiencing VIV for $m^* \to 0$ and m^*-$\zeta \to 0$ is still open and numerical simulations are expected to provide some insights on the matter since one can set $\zeta=0$ in numerical experiments; validation of numerical approaches is however a prerequisite, hence the numerous amount of numerical studies related to VIV at low mass-damping parameters.

To conclude with the general description of the coupled fluid-structure dynamics in VIV on circular cylinder it is worth describing the vortex shedding mode process which is associated with the cylinder response regime. Detailed experiments conducted by Govardhan & Williamson with DPIV (Digital Particle Image Velocimetry) have provided firm answers to questions raised by several authors regarding the relation between the cylinder response regimes and the vortex shedding mode [7]. Main features can be summed up as follows: Govardhan & Williamson have shown that i) the vortex shedding mode in the "initial branch" is characterized by the so-called "2S mode" according to the definition of Williamson & Roshko [27], in which two single vortices are shed downstream the cylinder during one period of oscillation (see Fig. 6, extracted from [7]), ii) the vortex shedding mode in the "upper" and "lower" branches is characterized by the so-called "2P mode", in which two pairs of vortices are shed downstream the cylinder during one period of oscillation (see Fig. 6); as indicated by the experimental visualizations, in the "upper branch", the "2P mode" is characterized by a vortex with high vorticity level and a second vortex with lower vorticity level and in the lower branch, the "2P mode" is characterized by vortices that stretch downstream, see Fig. 6 below.

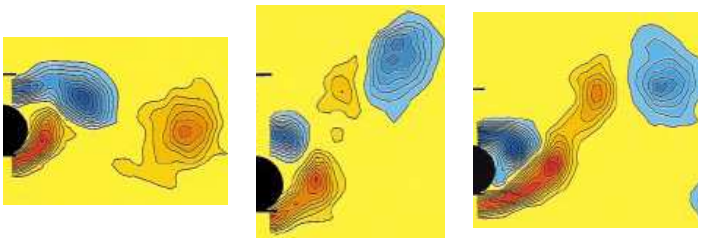

Initial branch — Upper branch — Lower branch
2S shedding mode — 2P shedding mode

Fig. 6. Vortex shedding mode (from Govardhan &Williamson, 2000 [7])

Numerical simulations conducted by several authors over the last years have provided interesting results which overall agree well with the experimental observations. However, reaching the "upper branch" response still remains a challenge: for instance, neither the 2D-FEM simulations of Singh & Mittal [22], nor the 3D-DVM simulations of Yamamoto et *al.* [28] or the 2D-FVM simulations of Placzek et *al.* [18] have been able to capture the "upper branch" response of the cylinder, even though other interesting features of VIV (such as hysteretic, three dimensional as well as low mass-damping effects) have been highlighted in these studies. As the "upper branch" regime is observed for moderate and high Reynolds numbers, and therefore appears as R_e-dependant, simulations have to account for turbulence phenomena; Al-Jamal & Dalton [1] performed 2D-LES simulations at R_e=8000, without however reaching the "upper branch", Guilmineau & Queutey [8] and Pan et *al.* [16] performed 2D-RANS simulations in a wide range of Reynolds numbers ($2000<R_e<10000$), which yielded promising results, since the "upper" branch regime was observed when using "U^*-increasing" conditions of simulations (i.e. by performing continuous simulations and gradually increasing the fluid upstream velocity – and the Reynolds number – while keeping all other parameters constant). However, the "upper branch" was not observed when using the "from rest" conditions (i.e. setting the fluid upstream velocity at a given value and letting the cylinder freely oscillate under VIV).

Purpose of the present paper is to investigate the numerical simulation of the VIV behavior of a rigid cylinder at low

mass-damping and moderate Reynolds numbers with a 2D[4] RANS CFD approach, using a "from rest" initial condition for the cylinder motion. As will be made conspicuous in the third section of the paper, our simulations have been able to predict a higher amplitude response for the cylinder in the "upper branch" regime with a "from rest" initial condition; to the authors' knowledge, such numerical results have not been reported yet. However, as will be detailed further on, our 2D RANS approach failed to capture the whole extent of the "upper branch" regime in terms of reduced velocity; the results are however encouraging and therefore worth publishing, even if complementary numerical investigations will be needed for further validations.

2. FLUID-STRUCTURE COUPLED SIMULATION OF VORTEX-INDUCED VIBRATION

In the present section, the basic principles of the coupled fluid-structure strategy for VIV simulation are discussed. The numerical procedure is rather classical for this class of coupled problems and lies on: i) finite volume CFD computations with RANS approach to consider a fluid flow at Reynolds numbers varying from 10^3 to 10^4 and ii) coupled fluid/structure procedures with fluid re-meshing technique to account for flow-structure interactions.

2.1. RANS approach for turbulent flow modeling with the k-ω SST model of Menter

Turbulent fluid flow is described through CFD computations with a numerical code equipped with RANS model (in the present case, the $k-\omega$ SST model of Menter [13]). The underlying modelling is recalled in what follows.
Conservation equations for incompressible fluid flow read:

$$\frac{\partial U_j}{\partial x_j} = 0 \tag{3}$$

$$\rho\left(\frac{\partial U_i}{\partial t} + U_j \frac{\partial U_i}{\partial x_j}\right) = -\frac{\partial P}{\partial x_i} + \mu \frac{\partial^2 U_i}{\partial x_j \partial x_j} \tag{4}$$

where (U_i) is the fluid velocity field and P is the fluid pressure field. Using the Reynolds decomposition, these latter fields are written as the sum of a mean and a fluctuating parts, i.e. $U_i = \overline{U_i} + u_i$ and $P = \overline{P} + p$, respectively (with $\overline{\bullet}$ standing for the mean part). Substituting the Reynolds decomposition in the Navier-Stokes equation yields the RANS equations :

$$\frac{\partial \overline{U}_j}{\partial x_j} = 0 \tag{5}$$

and:

$$\rho\left(\frac{\partial \overline{U}_i}{\partial t} + \overline{U}_j \frac{\partial \overline{U}_i}{\partial x_j}\right) = -\frac{\partial \overline{P}}{\partial x_i} + \mu \frac{\partial^2 \overline{U}_i}{\partial x_j^2} - \rho \frac{\partial \overline{u_i u_j}}{\partial x_j} \tag{6}$$

which account for the mean flow. Interaction of the fluctuating fields with the mean flow is accounted for through the Reynolds tensor:

$$\overline{u_i u_j} = -\tau\left(\frac{\partial U_i}{\partial x_j} + \frac{\partial U_j}{\partial x_i}\right) + \frac{2}{3} k \delta_{ij} \tag{7}$$

where τ stands for the turbulent viscosity and $k = \frac{1}{2}\overline{u_i u_i}$ is the turbulent kinetic energy. τ and k are to be calculated with an appropriate turbulence model. As made conspicuous further on, τ is calculated from the turbulent kinetic energy k and the turbulent dissipation ω. The $k-\omega$ SST model of Menter [14] combines a description of the turbulent shear layer (close to wall boundaries) with the standard $k-\omega$ model and a description of the turbulent flow (far from wall boundaries) with the $k-\varepsilon$ model. The $k-\omega$ SST model is therefore particularly well suited for RANS simulations of flows with adverse gradient pressure, as in the present case for VIV. Additional transport equations for the turbulent quantities k and ω are to be solved in conjunction with the equations of the mean flow:

- Transport equation for the turbulent kinetic energy

$$\frac{\partial k}{\partial t} + U_j \frac{\partial k}{\partial x_j} = \tau\left(\frac{\partial U_i}{\partial x_j} + \frac{\partial U_j}{\partial x_i}\right)\frac{\partial U_i}{\partial x_j} + \frac{\partial}{\partial x_j}\left((\nu + \frac{\tau}{\sigma_k})\frac{\partial k}{\partial x_j}\right) - \beta^* \omega k \tag{8}$$

- Transport equation for the turbulent dissipation

$$\frac{\partial \omega}{\partial t} + U_j \frac{\partial \omega}{\partial x_j} = \alpha\left(\frac{\partial U_i}{\partial x_j} + \frac{\partial U_j}{\partial x_i}\right)\frac{\partial U_i}{\partial x_j} - \beta\omega^2 + \frac{\partial}{\partial x_j}\left((\nu + \frac{\tau}{\sigma_\omega})\frac{\partial k}{\partial x_j}\right) + (1-F)\frac{2}{\sigma_\omega \omega}\frac{\partial k}{\partial x_j}\frac{\partial \omega}{\partial x_j} \tag{9}$$

with $\alpha = \frac{\beta}{\beta^*} - \frac{\kappa^2}{\sigma_\omega \sqrt{\beta^*}}$. Function F indicates whether the current location is "inside" the boundary layer ($F \to 1$) or "outside" the boundary layer ($F \to 0$); from the practical point of view, the SST model states that F is calculated according to $F = \tanh(\eta^4)$ where η is defined as $\eta = \min(\Delta, \frac{4k}{\sigma_\omega \psi^2} D)$, with $\Delta = \max(\frac{\sqrt{k}}{0.09\omega\psi}, \frac{500\nu}{\omega\psi^2})$,

[4] *VIV involves complex 3D phenomena that will be not correctly captured by 2D simulations. Apart from the obvious computational cost, 2D simulations can still be resorted with reasonable confidence in VIV simulations; Al-Jamal & Dalton give some physical argument which support (up to some extent) the physical signification of 2D modeling in VIV:* "2D calculation does allow for a reasonably accurate estimate of global parameters (…/…) when VIV begins since the correlation length increases significantly when VIV is established" *[1].*

$D = \max(\frac{2}{\sigma_\omega \omega}\frac{\partial k}{\partial x_j}\frac{\partial \omega}{\partial x_j}, 10^{-10})$ and ψ is the distance from the wall. The various coefficients of the model (see Eqs. [8] and [9]) are defined as follows:

$$\beta^* = \beta_\omega^* + (1-F)\beta_\varepsilon^*\,,\ \beta = \beta_\omega + (1-F)\beta_\varepsilon \qquad (10.a)$$

$$\sigma_k = \sigma_{k\omega} + (1-F)\sigma_{k\varepsilon}\,,\ \sigma_\omega = \sigma_{\omega\omega} + (1-F)\sigma_{\omega\varepsilon} \qquad (10.b)$$

and are specified in Tab. 2 below.

$\beta_\omega = 0.075$	$\beta_\varepsilon = 0.0828$	$\sigma_{k\omega} = 0.85$	$\sigma_{k\varepsilon} = 1$	$\kappa_\omega = 0.41$
$\beta^*{}_\omega = 0.09$	$\beta^*{}_\varepsilon = 0.09$	$\sigma_{\omega\varepsilon} = 1.168$	$\sigma_{\omega\omega} = 2$	$\kappa_\varepsilon = 0.41$

Tab. 2. Parameters of the k-ω SST model [14]

According to the SST model, the turbulent viscosity τ is calculated as:

$$\tau = \frac{ak}{\max(a\omega, \Omega G)} \qquad (10)$$

with $a = 0.31$, $G = \tan(\eta^2)$ and $\Omega = \sqrt{\Omega_{ii}^2}$, where Ω_{ij} is the vorticity tensor, defined as $\Omega_{ij} = \frac{1}{2}\left(\frac{\partial \overline{U}_i}{\partial x_j} - \frac{\partial \overline{U}_j}{\partial x_i}\right)$.

2.2. Finite volume method for CFD analysis

RANS simulations with the SST model consist in solving Eqs. (5), (6) and (7) together with the turbulent transport equations (8) and (9) and the turbulent viscosity model (10). In the present case, this is achieved with a CFD code based on the Finite Volume Method [6]. The computational domain is represented in Fig. 7(a) below: its dimensions are set-up in such manner to account for the unbounded configuration, i.e. to avoid blockage effects. Grid refinement is performed in the vicinity of the cylinder, as depicted by Fig. 7(b). A moving mesh procedure is employed to adjust the finite volume mesh to the cylinder motion and therefore account for flow-cylinder interactions. In order to save computational time, only a refined zone, represented in orange in Fig. 7(b), around the cylinder is handled with the dynamic mesh.

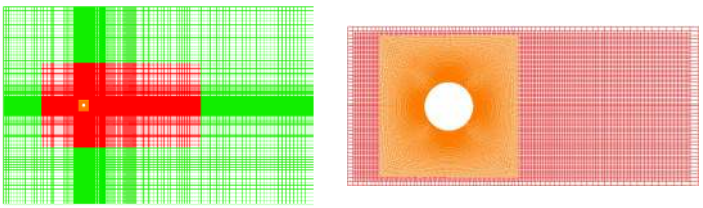

(**a**) Global CFD mesh (**b**) CFD mesh around the cylinder

Fig. 7. Finite volume mesh

The re-meshing algorithm is based on geometrical considerations and is designed in order to handle moderate mesh deformations around the cylinder [23]. Previous numerical studies on forced and free vibrations of a cylinder in this configuration have been extensively tested, which validate the procedure, see for instance Placzek et *al.* [17,18].

Since turbulent flow modeling is performed with a low-Reynolds type RANS model, no wall functions are used; the finite volume mesh has therefore to be such as the Y^+ value at the cylinder boundary should not exceed unity. Several mesh refinements are considered: as conveyed by Tab. 3 below, a mesh with 60 cells in the moving annular zone around the cylinder fulfills the requirement for a Reynolds number of 5000; this corresponds to a 27720 cell finite volume mesh of the computational domain, which is acceptable in order to perform numerous computations[5].

$N_{cylinder}$	35	45	50	*60*	70
N_{cells}	18720	22320	24120	*27720*	31320
Y^+	6.752	2.729	2.851	*0.970*	0.372

Tab. 3. Mesh refinement around the cylinder and corresponding Y^+ at the cylinder boundary for Re=5000

For a Reynolds number of 10000, the Y^+ value exceeds the unity limit in some locations around the cylinder but the criteria is overall respected (see Fig. 8); quality of the FV mesh will thus be considered as valid for the present study.

Fig. 8. Y^+ at the cylinder boundary for R_e=10000

To conclude with the general features of the numerical method for CFD computations, it is mentioned that discretization in space of Eqs. (5) to (10) is performed with the MARS scheme and discretization in time with the Crank-Nicholson scheme; the so-called PISO algorithm handles the pressure-velocity coupled equations through an implicit decoupling scheme [9,10].

2.3. Coupled fluid-structure calculation procedure

In the present paper, a coupled fluid-structure calculation procedure is used for VIV simulations. Either explicit [24] or implicit [25] methods can be used in coupled simulations; time integration of Eq. (1) is based here on an explicit algorithm [17,18,23,24], most suited than the implicit algorithm presented in [25]. Indeed, the numerical damping is

[5] *In the present study, CFD computations of VIV on the cylinder are performed with a "from rest" condition for the cylinder motion. Indeed, computation is re-started for each Reynolds number (and each reduced velocity); This approach is much more demanding in terms of computational time than the strategy resorted to by Guilmineau & Queutey [8] and Pan et* al. *[16], who both used an "increasing" condition, for which computations were performed in a continuous manner with increment on the Reynolds number (reduced velocity).*

dramatically reduced by combining a centered upwind and downwind discretization scheme for the prediction of the displacement.

The steps of the algorithm write:

1. Initialization for the first iteration

$$y^n = y_0 \quad \dot{y}^n = \dot{y}_0 \quad \ddot{y}^n = \ddot{y}_0 \quad \varphi_L^n = \phi_0$$

2. Evaluation of the cylinder acceleration

$$\ddot{y}^{n+1} = \frac{\varphi_L^n}{m} - \frac{k}{m} y^n - \frac{c}{m} \dot{y}^n$$

3. Evaluation of the cylinder velocity and displacement

$$\dot{y}^{n+1} = \dot{y}^n + \delta t \, \ddot{y}^{n+1}$$

$$y^{n+1} = y^n + \delta t \left[(1-\theta) \dot{y}^n + \theta \dot{y}^{n+1} \right]$$

4. Resolution of the flow field with the CFD code to obtain φ_L^{n+1}
5. Return to step 2 (next time step)

The procedure is implemented in a user subroutine read by the CFD code at each time step before solving the flow field. Several numerical tests performed in [17,23] have shown that $\theta = 0.5$ gives the smallest numerical damping for a perfect flow; the coupled method has also been extensively tested in the case of VIV at low Reynolds number [18] and therefore validated for the problem of concern here.

3. NUMERICAL RESULTS AND DISCUSSION

Numerical calculations are performed at low mass ratio (m^*~2.4) and low mass-damping ratio ($m^*\zeta$~0.014), which corresponds to the conditions of experiments in Khalak & Williamson [11,12] and of computations in Guilmineau & Queutey [8] and Pan et *al.* [16].

Simulations are performed for increasing values of U^* (or R_e), starting with "from rest" conditions of motion for the cylinder in a range of reduced velocities which extends from U^*~1 to U^*~17, i.e. R_e varying from 10^3 to 10^4.

Response of the cylinder undergoing VIV is analyzed in terms of amplitude and frequency of oscillations, as well as of vortex shedding modes.

3.1. Amplitude of oscillations

Figures 9.a to 9.d give time histories of the cylinder transverse motion, with different reduced velocities. Each of the situations can be related to a) the initial branch (U^*=3.75), b) the upper branch (U^*=4.45), c) the lower branch (U^*=6.85) and d) the desynchronization regime (U^*=13.75).

At U^*=3.75, features of the cylinder response are characteristic of the initial branch (aperiodic response, with a maximum amplitude A^*~0.52). Times histories of Fig. 9.a show identical trends as those highlighted by Guilmineau & Queutey for U^*=3.63 (see Fig. 2.(b) in [8]). At U^*=4.45, the response of the cylinder seems of upper branch-type, according to the description of Khalak & Williamson recalled in the first section: the cylinder vibration amplitude reaches A^*~0.77 and drops to A^*~0.60: this can be interpreted as a switch between the upper and lower branches, which seems to be captured by the RANS approach: A^*~0.8 could therefore be interpreted as a mean value between A^*=0.6 in the lower branch and A^*=1.0 in the upper branch.

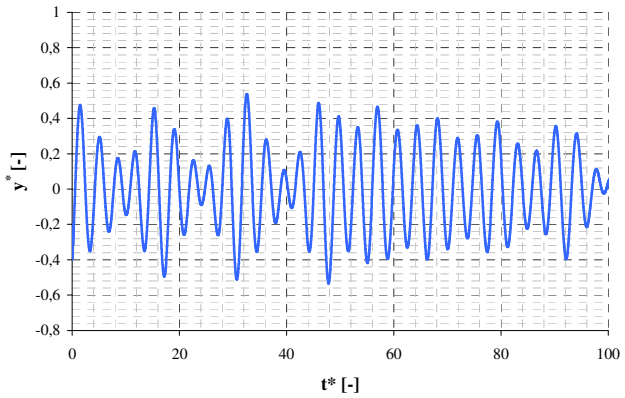

Fig. 9.a. Cylinder oscillations for R_e=2750 – U^*=3.75 (initial excitation)

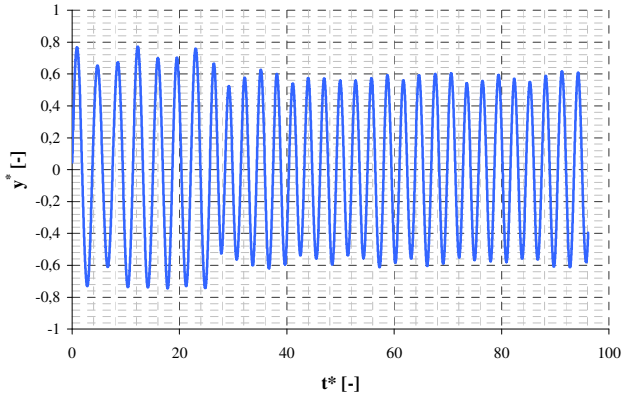

Fig. 9.b. Cylinder oscillations for R_e=3250 – U^*=4.45 (upper branch)

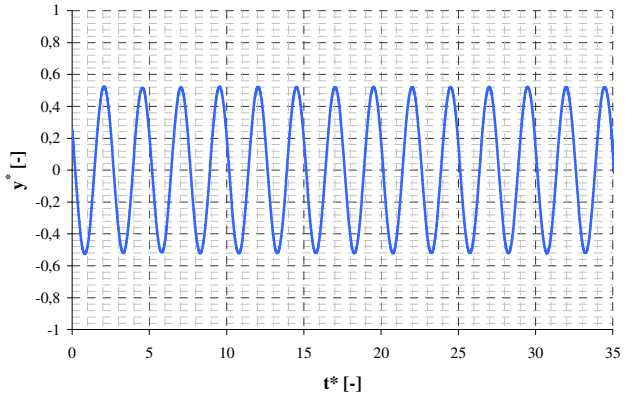

Fig. 9.c. Cylinder oscillations for R_e=5000 – U^*=6.85 (lower branch)

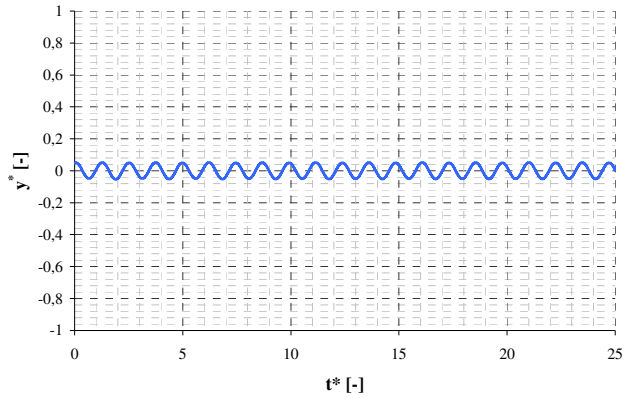

Fig. 9.d. Cylinder oscillations for R_e=10000 – U^*=13.75 (desynchronization)

Time histories in Fig. 9.b are similar to those obtained by Guilmineau & Queutey for U^*=4.37 (see Fig. 4.(a) in [8]).
At U^*=6.85, the cylinder response exhibits a perfect sinusoid with amplitude A^*~0.52, which is consistent with the lower branch type response.

Figure 9.c gives similar trends as those observed by Guilmineau & Queutey (see Fig. 2.(e) in [8]) and Pan et *al.* (see Fig. 3 in [16]). At U^*=13.75, the cylinder response is periodic with low amplitude motions (A^*~0.05): desynchronization is reached; plots of Fig. 9.d are quite identical with those presented by Guilmineau & Queutey in the desynchronization regime (see Fig. 2.(h) in [8]).

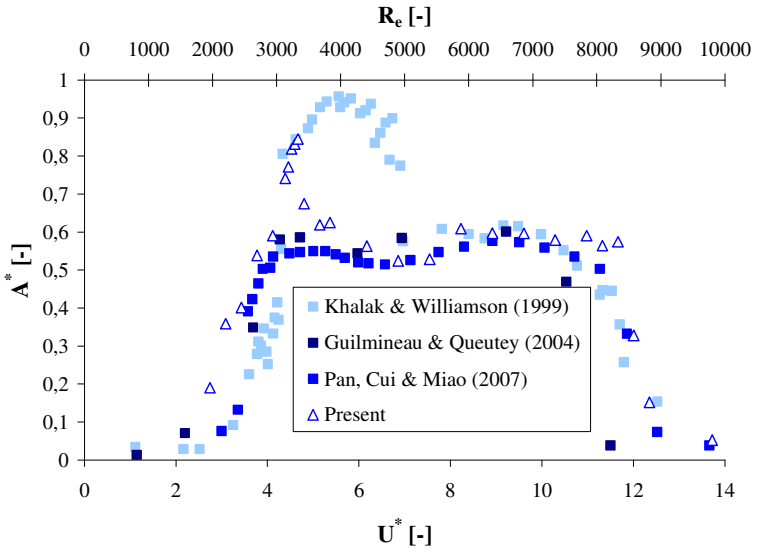

Fig. 10. Amplitude of cylinder vibration under vortex shedding

Figure 10 gives the maximum amplitude A^* computed throughout the reduced velocity range $1<U^*<17$ and compares the present numerical results with the experiments of Khalak & Williamson [11,12] and with the computations in Guilmineau & Queutey [8] and Pan et *al.* [16][6].

Quantitative agreement of our numerical results, when compared to the preceding experiments and computations, is observed as far as the initial branch, lower branch and synchronization range are concerned. Qualitative agreement of our numerical results with the experiments is observed as far as the upper branch is concerned. Amplitude response of the cylinder around A^*~0.85 is obtained for a reduced velocity about U^*~4.65, but the extent of this higher amplitude zone is rather narrow when compared to the experiments. However, the present numerical results are rather promising since no similar trend has been observed with VIV simulations based on a "from rest" initial condition.

3.2. Cylinder oscillating frequency

Figure 11 gives the evolution of the frequency ratio f^* of the cylinder oscillations throughout the reduced velocity range $1<U^*<17$ and compares the present numerical results with the experiments of Khalak & Williamson [11,12] and with the computations in Guilmineau & Queutey [8] and Pan et *al.* [16].

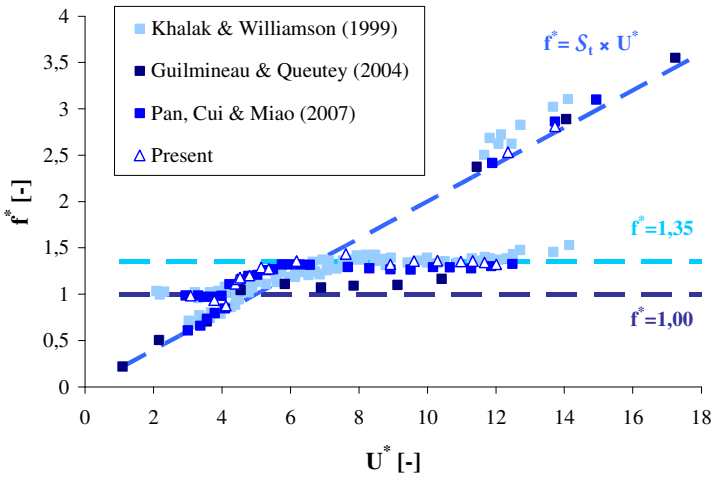

Fig. 11. Oscillation frequency of cylinder vibration under vortex shedding

The present numerical simulations are in very good agreement, both from the quantitative and qualitative points of view, with the preceding experiments and simulations; in particular, the frequency ratio remains constant at value f^*=1.35 throughout the synchronization regime, which is in agreement with the experiments of Khalak & Williamson for low mass-damping cylinders.

[6] *In computations of Guilmineau & Queutey and Pan et* al.*, only the "from rest" conditions are considered. Higher amplitude responses have been obtained by these authors with the "increasing" condition. For the sake of comparison, only the "from rest" computation results are presented here since it corresponds to our numerical approach.*

3.3. Vortex shedding modes

Figures 12.a to 12.c give the computed vorticity contours in the fluid at various positions of the cylinder and for various flow conditions.

At R_e=2750 (U^*=3.75), the vortex shedding mode is clearly of 2S-type: a single pair of vortices is shed during a period of oscillation of the cylinder, which is characteristic of the initial branch response.

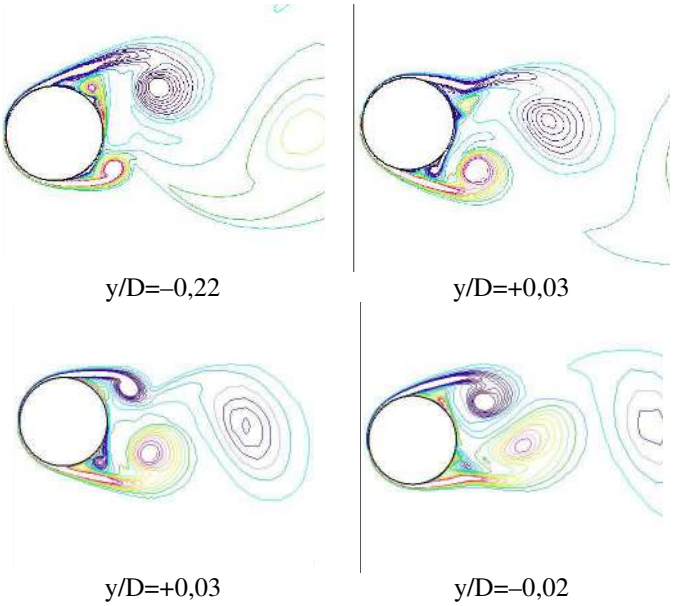

y/D=–0,22 y/D=+0,03

y/D=+0,03 y/D=–0,02

Fig. 12.a. Vortex shedding modes at R_e=2750 (initial branch)

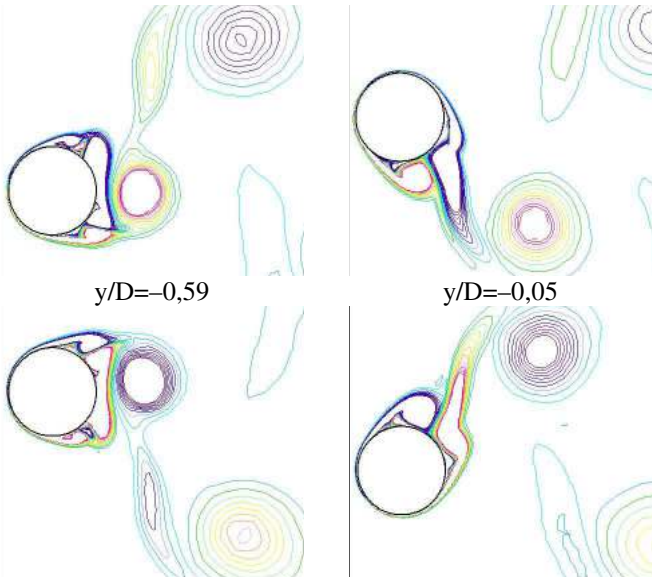

y/D=–0,59 y/D=–0,05

y/D=+0,63 y/D=–0,08

Fig. 12.b. Vortex shedding modes at R_e=3250 (upper branch)

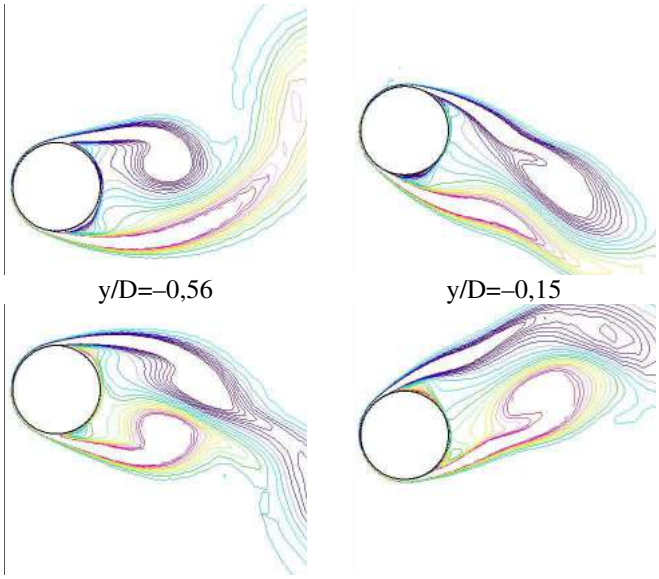

y/D=–0,56 y/D=–0,15

y/D=+0,55 y/D=–0,01

Fig. 12.c. Vortex shedding modes at R_e=5000 (lower branch)

The simulated flow pattern is similar to the observed pattern in the experiments of Govardhan & Williamson (see Fig. 6 above, and Fig. 11 in [7]) as well as in the computations of Pan et *al*. (see Fig. 5 in [16]). At R_e=3250 (U^*=4.45), the vortex shedding mode is obviously of 2P-type, two pairs of vortices being shed during one oscillation cycle of the cylinder, which is experimentally observed by Govardhan & Williamson (see Fig. 6 above, and Fig. 12 in [7]) and evidences the upper branch response.

The simulated flow pattern is similar to the one obtained by Pan et *al*. with "increasing" initial conditions for equivalent flow conditions (see Fig. 6 in [16]). At R_e=5000 (U^*=6.85), the vortex shedding mode is 2P-like: two pairs of vortices are shed downstream the cylinder, but a merging/stretching process is observed, in which the vortex with higher activity somehow "swallows" the vortex with lower activity. Our simulations are consistent with the experimental and numerical observations of Govardhan & Williamson on the one hand (see Fig. 6 above and Fig. 13 in [7]) and of Pan et *al*. on the other hand (see Fig. 7 in [16]).

CONCLUSION

Numerical simulation of the VIV response of a cylinder freely vibrating transversely to a fluid flow at moderate Reynolds numbers (10^3 to 10^4) has been performed in the present study under low mass-damping conditions.

Simulations have been performed using a coupled CFD/CDS procedure, with a 1-DOF modeling for the structure and RANS modeling for the fluid.

Numerical results have been exposed and compared with experiments of Khalak & Williamson (1997), Govardhan &

Williamson (2000) on the one hand and simulations of Guilmineau & Quetey (2004), Pan, Cui & Miao (2007) on the other hand. Quantitative agreement has been highlighted as far as the cylinder oscillation amplitude and frequency is concerned; quantitative agreement has also been observed in the vortex shedding patterns.

Furthermore, the presented numerical simulations yield the "upper branch" response with "from rest" initial conditions, which has never been reported so far in CFD computations. The simulations results are therefore very encouraging, in particular from the engineering point of view, since the proposed coupled analysis can be considered as valid for practical applications. Application of the coupled analysis in tube bundle configuration is in such context under consideration.

Further investigations of the problem will be devoted to CFD computations with LES or DNS, as well as ROM approaches and will be presented in future communications.

REFERENCES

[1] H. AL-JAMAL, C. DALTON. Vortex Induced Vibrations Using Large Eddy Simulation at a Moderate Reynolds Number. *Journal of Fluids and Structures*, **19**, 73-92, 2004.

[2] R.D. BLEVINS. *Flow-Induced Vibrations*. Van Nostrand Reinhold, 1990.

[3] S.S. CHEN. *Flow Induced Vibrations of Circular Cylindrical Structures*. Hemisphere Publishing Corporation, 1987.

[4] S. DONG, G.E. KARNIADAKIS. DNS of Flow Past a Stationary and Oscillating Circular Cylinder at Re=10000. *Journal of Fluids and Structures*, **20**, 519-531, 2005.

[5] C.C. FENG. *The measurement of vortex-Induced Effects Past Stationary and Oscillating Cricular and D-Section Cylinders*. Master's Thesis, University of British Columbia, 1968.

[6] J.H. FERZIGER, M. PERIC. *Computational Methods for Fluid Dynamics*. Springer-Verlag, 1996.

[7] R. GOVARDHAN, C.H.K. WILLIAMSON. Modes of Vortex Formation and Frequency Response of a Freely Vibrating Cylinder. *Journal of Fluid Mechanics*, **420**, 85-130, 2000.

[8] E. GUILMINEAU, P. QUEUTEY. Numerical Simulation of Vortex-Induced Vibration of a circular Cylinder with Low Mass-Damping in a Turbulent Flow. *Journal of Fluids and Structures*, **19**, 449-466, 2004.

[9] R.I. ISSA. Solution of the Implicitly Discretised Fluid Flow Equations by Operator Splitting. *Journal of Computational Physics*, **62**, 40-65, 1986.

[10] R.I. ISSA, A.D. GOSSMAN, A.P. WATKINS. The Computation of Compressible and Incompressible Recirculating Flows. *Journal of Computational Physics*, **62**, 519-531, 1986.

[11] A. KHALAK, C.H.K. WILLIAMSON. Fluid Forces and Dynamics of a Hydroelastic Structure With Very Low Mass-Damping. *Journal of Fluids and Structures*, **11**, 973-982, 1997.

[12] A. KHALAK, C.H.K. WILLIAMSON. Motions, Forces and Mode Transitions in Vortex-Induced Vibrations at Low Mass Damping. *Journal of Fluids and Structures*, **13**, 813-851, 1999.

[13] F.R. MENTER. *Zonal Two-Equations k-ω Turbulence Model for Aerodynamics Flows*, AIAA Paper 93-2906, July 1993.

[14] F.R. MENTER. Two-Equations Eddy-Viscosity Turbulence Models for Engineering Applications. *AIAA Journal*, **32** (8), 1598-1605, 1994.

[15] S. MITTAL, V. KUMAR. Flow-Induced Vibrations of a Light Circular Cylinder at Reynolds numbers 10^3 to 10^4. *Journal of Sound and Vibration*, **245** (5), 923-946, 2001.

[16] Z.Y. PAN, W.C. CUI, Q. M. MIAO. Numerical Simulation of Vortex-Induced Vibration of a Circular Cylinder at Low mass-Damping Using RANS Code. *Journal of Fluids and Structures*, **23**, 23-37, 2007.

[17] A. PLACZEK, J.F. SIGRIST, A. HAMDOUNI. *Numerical Simulation of Vortex Shedding Past a Circular Cylinder at Low Reynolds Number with Finite Volume Technique. Part I: Forced Oscillations*. Pressure Vessel and Piping. San Antonio, 22-26 July 2007.

[18] A. PLACZEK, J.F. SIGRIST, A. HAMDOUNI. *Numerical Simulation of Vortex Shedding Past a Circular Cylinder at Low Reynolds Number with Finite Volume Technique. Part II: Flow Induced Vibrations*. Pressure Vessel and Piping. San Antonio, 22-26 July 2007.

[19] T. SARPAKAYA. Vortex-Induced Oscillations: a Selective Review. *Journal of Applied Mechanics*, **46**, 421-258, 1979.

[20] H. SCHLICHTING, K. GERSTEN. *Boundary L ayer Theory*, Springer, 2000.

[21] D. SHIELS, A. LEONARD, A. ROSHKO. Flow-Induced Vibration of a Circular Cylinder at Limiting Structural Parameters. *Journal of Fluid and Structures*, **15**, 3-21, 2001.

[22] S. P. SINGH, S. MITTAL. Vortex-Induced Vibration at Low Reynolds Numbers: Hysteresis and Vortex-Shedding Modes. *Journal of Fluids and Structures*, **20**, 1085-1104, 2005.

[23] J.F. SIGRIST. *Modélisation et simulation numérique d'un problème couplé fluide/structure non-linéaire. Application au dimensionnement de structures nucléaires de propulsion navale*. Ph.D Thesis, Université de Nantes, 2004.

[24] J.F. SIGRIST, C. LAINE, B. PESEUX. *Numerical Simulation of a Non Linear Coupled Fluid-Structure Problem by Explicit Finite Element-Finite Volume Coupling*. Pressure Vessel and Piping, Denver, 17-21 July 2005.

[25] J.F. SIGRIST, D. ABOURI. *Numerical Simulation of a Non-Linear Coupled Fluid-Structure Problem with Implicit and Explicit Coupling Procedures*. Pressure Vessel and Piping, Vancouver, 25-28 July, 2006.

[26] B.S. VARAPRASAD PATNAIK, A. ASWATHA NARAYANA, K.N. SEETHARAMU. Numerical Simulation of Laminar Flow Past a Transversely Vibrating Circular Cylinder. *Journal of Sound and Vibration*, **228**, 459-475, 1999.

[27] C.H.K. WILLIAMSON, A. ROSHKO. Vortex Formation in the Wake of an Oscillating Cylinder. *Journal of Fluids and Structures*, **2**, 355-381, 1988.

[28] C.T. YAMAMOTO, J.R. MENEGHINI, F. SALTARA, R.A. FREGONESI, J.A. FERRARI. Numerical Simulation of Vortex-Induced Vibration on Flexible Cylinders. *Journal of Fluids and Structures*, **19**, 467-489, 2004.